Journal of Alloys and Compounds 509 (2011) 10190–10194

Contents lists available at ScienceDirect

Journal of Alloys and Compounds

journal homepage: www.elsevier.com/locate/jallcom

Transparent conducting oxide films of heavily Nb-doped titania by reactive co-sputtering

Kai-Hsiang Hung, Pei-Wei Lee, Wei-Chun Hsu, Hsiang Chun Hsing, Hsiao-Tzu Chang, Ming-Show Wong*

Department of Materials Science and Engineering, National Dong Hwa University, Hualien, Taiwan

ARTICLE INFO

Article history:
Received 9 February 2011
Received in revised form 3 August 2011
Accepted 4 August 2011
Available online 11 August 2011

Keywords:
Titania
Nb doped TiO_2
Anatase
Rutile
Transparent conducting oxide

ABSTRACT

Niobium-doped titania (TNO) films of various Nb content were deposited on glass and silicon substrates by reactive co-sputtering of Ti and Nb metal targets. Nb content in the TNO films was varied from 0 to ~13 at.% (atomic percent), corresponding to $Ti_{1-x}Nb_xO_2$ with x = 0–0.52, by modulating the Nb target power from 0 to 150 W (Watts). The influence of ion bombardment on the TNO films was investigated by applying an RF substrate bias from 0 to 25 W. The as-deposited TNO films were all amorphous and insulating, but after annealing at 600 °C for 1 h in hydrogen, they became crystalline and conductive. The annealed films crystallized into either pure anatase or mixed anatase and rutile structures. The as-deposited and the annealed films were transparent, with an average transmittance above 70%. Anatase TNO film ($Ti_{1-0.39}Nb_{0.39}O_2$) with Nb 9.7 at.% exhibited a dramatically reduced resistivity of 9.2×10^{-4} Ω cm, a carrier density of 6.6×10^{21} cm^{-3} and a carrier mobility around 1.0 $cm^2 V^{-1} s^{-1}$. In contrast, the mixed-phase $Ti_{1-0.39}Nb_{0.39}O_2$ showed a higher resistivity of 1.2×10^{-1} Ω cm. This work demonstrates that the anatase phase, oxygen vacancies, and Nb dopants are all important factors in achieving high conductivities in TNO films.

1. Introduction

Transparent conducting oxide (TCO) films have found a wide range of industrial applications in recent years. Flat-panel displays, light-emitting devices, and photovoltaic cells all use TCO [1]. Indium tin oxide (ITO) is the most commonly used TCO due to its low resistivity of approximately 2×10^{-4} Ω cm and high visible transmittance of 90% [2]. However, ITO cannot preserve high conductivity when it operates at high temperature (>400 °C) [3]. Also, indium element has limited availability. These drawbacks restrict ITO applications subsequently.

As an abundant, innocuous and chemically stable materials, titania (TiO_2) films have many practical functions, including photocatalysis, ferromagnetism, and solar cells [3–7]. TiO_2 exists primarily in three polymorphs: anatase, rutile, and brookite, each having different crystal structures and physical properties. It has recently been reported that doped anatase TiO_2 film is an attractive candidate for TCOs. The dopants in TiO_2-based TCOs include Nb [8–10], Ta [11], and W [12]. Nb-doped TiO_2 (denoted as $Ti_{1-x}Nb_xO_2$ or TNO) films reveal as excellent transparent conducting behaviors as ITO [8]. Based on its excellent chemical stability and enhanced conductivity, TNO films have been operated as either conductive electrodes [3,13] or photoanodes [14,15] for dye-sensitized solar cells successfully.

Numerous relevant papers describe both epitaxial [16–18] and polycrystalline [9,19] TNO films as TCOs using either PLD or sputtering methods. TNO films with $x \sim 0.05$ are now widely held to be the most prominent TiO_2-based TCO films, and TNO films with Nb content below ~5% as TCO have been reported in many publications [8,9,17–19]. However, the study of TNO films of high Nb content ($x > 0.05$) as TCO is rare. TNO films made of rutile or mixed anatase and rutile phase are paid less attention as well. Effect of Nb dopant on TiO_2 crystal structures is an essential factor [20,21]. For example, Nb dopants can generate electron carriers and profit conductivity of TNO films, while excess dopants could induce lattice deformation or additional phases such as Nb_2O_5 and $TiNb_2O_7$. The aim of the present paper is to investigate the influence of composition and structure of TNO films ($x > 0.05$) on their electro-optical properties. By reactive sputtering technique, chemical stoichiometry and crystal structures of films can be effectively controlled through modulating substrate bias to improve the kinetic energy of plasma species. Here, we report the electrical, optical, and structural properties of TNO (x = 0–0.52) polycrystalline films formed by co-sputtering method. Relationship between electric-optical properties and TNO structures, including pure anatase or mixed anatase and rutile structures, is discussed.

* Corresponding author.
E-mail address: mswong@mail.ndhu.edu.tw (M.-S. Wong).

0925-8388/$ – see front matter © 2011 Elsevier B.V. All rights reserved.
doi:10.1016/j.jallcom.2011.08.020

2. Experimental

Polycrystalline TNO films were fabricated on Corning 1737 glass and silicon substrates by reactive co-sputtering of three pure titanium and one niobium metal targets in argon and oxygen plasma using a pent-cathode magnetron sputtering system (AJA Inc. Mass, USA). The substrates were sputter-etched with argon ions (Ar^+) for 10 min prior to film deposition to remove any residual pollutants on the surface. Three sputtering guns, set at 200 W DC (direct-current), were used for the Ti target. A single gun was used for the Nb target, and its power was variably set at 0, 90, 105, 120, 135, and 150 W RF (radio frequency) for respective samples. The distance between the target surface and substrate holder was 100 mm. Working pressure was fixed at 0.4 Pa and the substrates were held at 350 °C with a 5 rpm rotation. The film deposition time was 30 min. A series of TNO films with varying Nb content were prepared by modulating the Nb target RF-power in a range from 90 to 150 W, while the oxygen gas flow was fixed at 9 sccm. Another series of TNO films were sputtered at various substrate bias power levels in the range from 0 to 25 W RF, while the Nb target power was fixed at 120 W RF.

The as-deposited films were post-annealed in natural air at 101 kPa and in hydrogen at 111 kPa at 600 °C for 1 h, respectively. The heating rate was 10 °C/min. The optical and electrical properties were obtained from the films deposited on glass substrates, while the other characterizations were done on the films on silicon. Film structure was characterized using a Rigaku D/Max-2500 18 kW X-ray diffractometer (Rigaku Corporation, Tokyo, Japan) using Cu Kα radiation at 40 kV and 150 mA, and a 3° incident angle. Film composition was estimated by a Thermo K-Alpha X-ray photoelectron spectrometer (Thermo Fisher Scientific Inc., MA, USA). UV–visible spectra of the films were obtained using a Hitachi 3300H spectroscope (Hitachi, Ltd., Tokyo, Japan), with a scanning wavelength of 200–1000 nm. The film electrical transport properties, including resistivity, carrier density, and Hall mobility, were determined by a Hall measurement system (Accent HL5500PC, Nanometrics, Inc., Ontario, Canada) at room temperature, as well as under a temperature range between 20 K and 300 K.

3. Results and discussion

Fig. 1 shows film deposition rate versus Nb target power of a series of TNO films prepared by modulating the Nb target RF power from 0 and 90 to 150 W. The deposition rate for pure titania film was 1.1 nm/min. The increase of Nb target power from 90 to 150 W caused a steep increase in the deposition rate, to 2.2 nm/min. One reason for this observation is that Nb has a sputtering yield (0.7) higher than that of Ti (0.5). Another factor may be due to poisoning of the metal targets when oxygen flow exceeded a critical value. The Nb target, sputtered by RF power, experienced less target poisoning than the Ti targets, sputtered by DC power under a reactive oxygen-argon atmosphere. Film thickness increased from 33 nm to 64 nm with the increase of the Nb target power from 0 to 150 W.

The as-deposited pure titania film was of poor crystallinity containing anatase, and the doped TNO films were all amorphous, since the films were deposited at a low substrate temperature. The difference in valence electrons and ionic size of Ti and Nb as well as the relative metal–oxygen bond lengths of Ti and Nb oxides could also contribute to the dopant-induced amorphization. The pure titania and the as-grown TNO films crystallize into the anatase structure after H_2-heat treatment at 600 °C for 1 h as shown in Fig. 2. Strong anatase-preferred orientation (1 0 1) was observed in the post-annealed films and the (1 0 1) peak position shifted to lower angular side with increasing Nb sputtering power, indicating lattice expansion due to the incorporation of Nb in the films. As Nb sputtering power exceeded 120 W, the crystallinity of TNO film was diminished. The (1 0 1) peak was weakened, and the film structure was converted to anatase (0 0 4) with poor crystallinity. The variations of crystallinity reflected on films conductivity are elaborated accordingly in the films conductivity results.

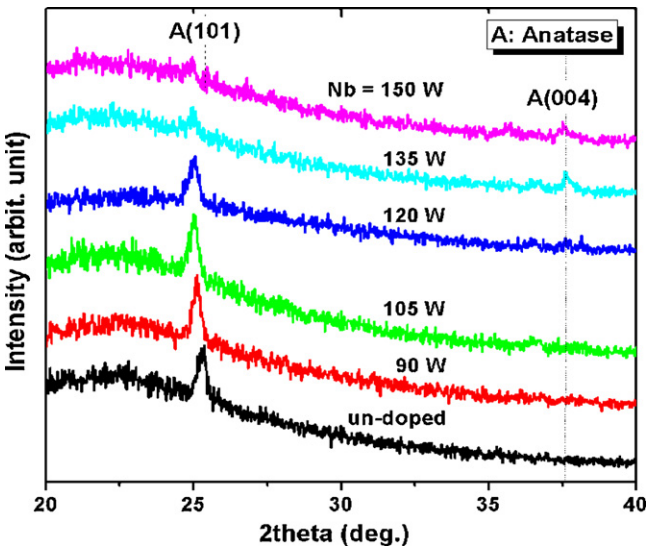

Fig. 2. X-ray diffraction patterns of the H_2-annealed TNO films.

The chemical compositions of the annealed TNO films determined by XPS analysis are shown in Fig. 3. An additional *y*-axis on right side of Fig. 3 is added for Nb ratio or Nb/(Ti + Nb)%. As Nb target power is increased from 90 to 150 W, the Nb metal content in the films increases almost linearly from 6.9 to 13 at.%, while the Ti content decreases from 20 to 12 at.%. The oxygen contents fluctuated slightly above 70 at.%. In fact, Nb content in TNO could be greater than 40 at.% of the metal component, and the TNO still maintained an anatase phase [21]. Sheppard et al. concluded that charge compensation occurs by the formation of cation vacancies, and by

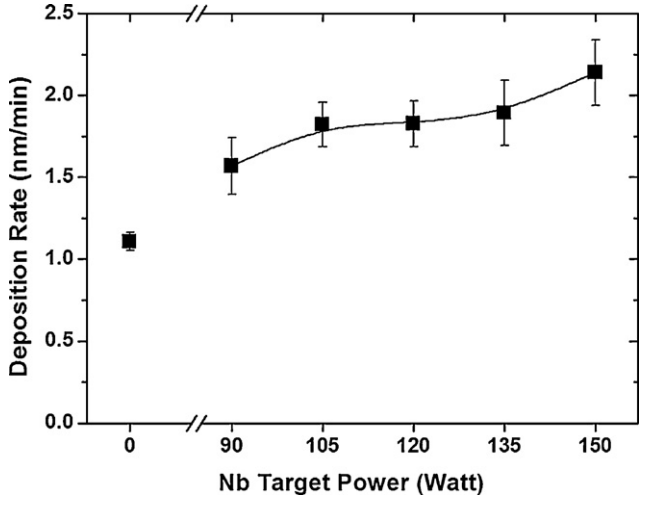

Fig. 1. Deposition rate of the TNO films as a function of Nb target power.

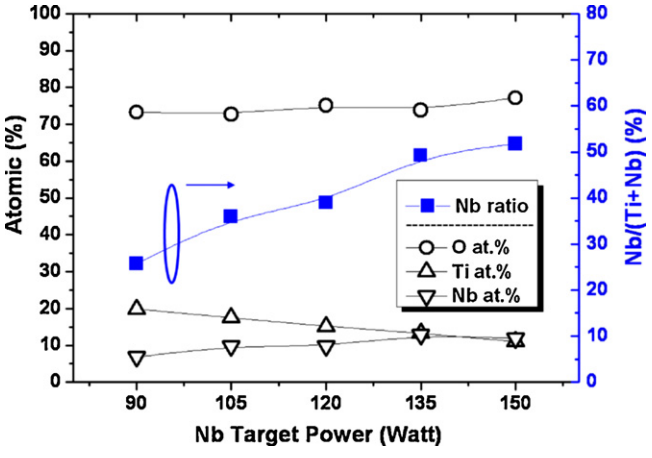

Fig. 3. Chemical composition (left *y*-axis) and the Nb ratio (right *y*-axis) of the H_2-annealed TNO films versus Nb target power.

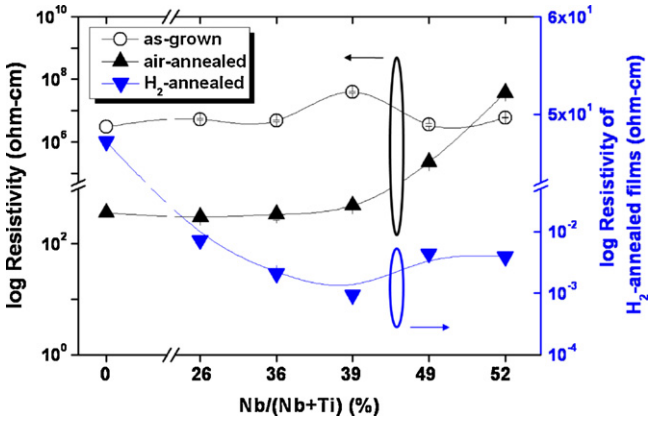

Fig. 4. Electrical resistivity of the TNO films versus Nb ratio.

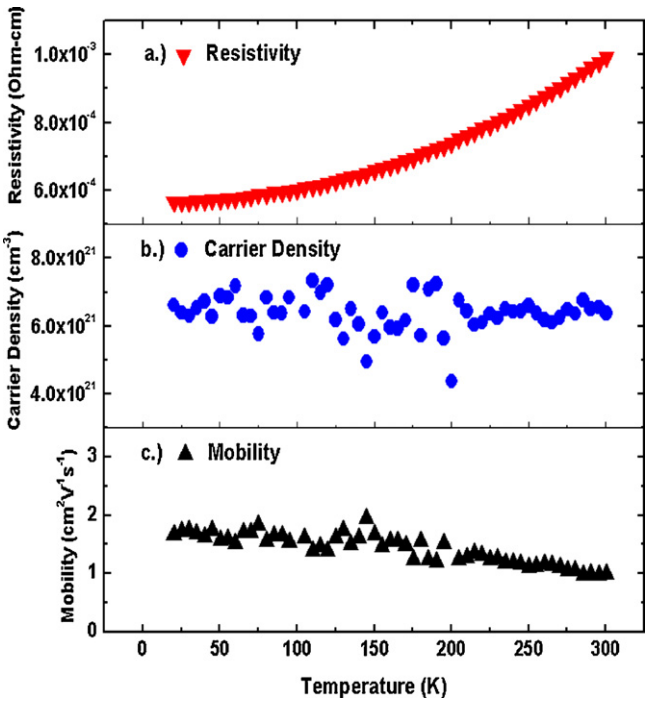

Fig. 5. Temperature dependence of (a) resistivity, (b) carrier density, and (c) Hall mobility for the H_2-annealed $Ti_{1-0.39}Nb_{0.39}O_2$ film.

reduction of Ti^{4+} to Ti^{3+} ions and/or Nb^{5+} to Nb^{4+} ion, depending on the Nb concentration in the film [21]. When high concentration of dopant is incorporated, the TiO_2 matrix could accompany the formation of fully oxidized niobium pent oxide which contains up to 71% oxygen. Accordingly, the ratio between O and metallic (Nb + Ti) in TNO films could be greater than 2. The annealed TNO films in this study preserve anatase structure, the chemical formula of $Ti_{1-x}Nb_xO_2$ is assumed. Thus, the series of films prepared can be depicted as $Ti_{1-x}Nb_xO_2$ with $x = 0.25$–0.52 in this study.

Fig. 4 illustrates how annealing the TNO films in air and in hydrogen, dramatically alters electrical conductivities of these films. The as-deposited TNO films presented the insulating behavior with resistivity of above $1 \times 10^6\ \Omega$ cm, since they were all amorphous. Annealed in an air environment, the amorphous TNO films (for Nb ratio ≦39%, i.e. Nb target ≦120 W) crystallized into anatase and had a decreased resistivity about $3 \times 10^2\ \Omega$ cm. For the TNO films of high Nb ratio over 49%, the air-annealed films became amorphous with high resistivity of above $2 \times 10^5\ \Omega$ cm. The crystallization from amorphous to anatase under the air atmosphere improved the conductivity for TNO films with Nb ratio <39%. In contrast to the air-annealed TNO films, the conductivity of TNO films improved markedly through H_2 annealing. On the right side of Fig. 4, an additional *y*-axis in different scale is presented to the doping effect on resistivity for the H_2-annealed films. For the H_2-annealed un-doped films, the resistivity reduced from $3.0 \times 10^6\ \Omega$ cm decreasing to $4.7 \times 10^1\ \Omega$ cm, about five orders of magnitude smaller than that of as-grown films. Indeed, conductivity of H_2-annealed films was further enhanced by incorporating the Nb dopant. The values of resistivity for the H_2-annealed doped films varied between 10^{-2} and $10^{-4}\ \Omega$ cm, with a high carrier density of about 2–$7 \times 10^{21}\ cm^{-3}$ and mobility in the range from 0.4 to $1\ cm^2\ V^{-1}s^{-1}$. While the Nb ratio increased from 26% to 39%, the resistivity of TNO film was decreased from $7.2 \times 10^{-3}\ \Omega$ cm to a minimum value of $9.2 \times 10^{-4}\ \Omega$ cm. The minimum resistivity increased to about $4 \times 10^{-3}\ \Omega$ cm, while the Nb ratio of the TNO films is over 39%. The attenuated conductivity could be caused by the poor crystalline anatase (1 0 1) of excess Nb doped TNO films, as demonstrated in Fig. 2. As Nb ratio equals to 39%, the H_2-annealed TNO film, a crystalline anatase phase, exhibits the minimum resistivity of $9.2 \times 10^{-4}\ \Omega$ cm.

In addition to the crystalline phase of anatase, Nb dopants and oxygen vacancies are also important factors in achieving high conductivity in TNO films. First, the ionized impurity, Nb^{5+}, acts as a shallow donor and generates carrier electrons with an ionization efficiency of up to 80% due to the Nb^{5+} ion's small ionic radius of 0.78 Å, which is similar to that of the Ti^{4+} ion at 0.75 Å in an octahedral coordination [19,22]. As such, the Nb ions are highly soluble in Ti sites and release free electrons with a high efficiency in the crystalline anatase TiO_2 structure [8,19]. The other factor for improving conductivity of TNO films could be oxygen vacancies. Annealing TNO films in air triggered the anatase phase (for Nb ratio≦39%), but it only reduced the film resistivity from $1 \times 10^6\ \Omega$ cm to $4 \times 10^2\ \Omega$ cm ($Ti_{1-0.39}Nb_{0.39}O_2$). The magnitude of reduction was much less than that of the H_2-treated films. In fact, post-annealing under a strongly reducing environment may induce oxygen deficiency or oxygen vacancies in TiO_2, and generates more carrier electrons to improve conductivity. Thus, the resistivity of H_2-annealed TNO films was lower than that of the air-annealed TNO films although they are all crystalline anatase.

The H_2-annealed $Ti_{1-0.39}Nb_{0.39}O_2$ films exhibited the minimum resistivity ($9.2 \times 10^{-4}\ \Omega$ cm) among all the studied samples (Fig. 4). Therefore, it was chosen for the study of the temperature dependence of resistivity, carrier density, and Hall mobility, depicted in Fig. 5. The film resistivity versus temperature curve in Fig. 5a shows a positive slope, indicating metallic behavior. The resistivity increases from $5.6 \times 10^{-4}\ \Omega$ cm at 20 K to $9.2 \times 10^{-4}\ \Omega$ cm at 300 K. Fig. 5b exhibits an n-type carrier density at around $6.6 \times 10^{21}\ cm^{-3}$, which is essentially independent of the temperature. The temperature dependent carrier mobility is shown in Fig. 5c. The mobility falls gradually with increasing temperature, from $1.6\ cm^2\ V^{-1}\ s^{-1}$ at 20 K to $1.0\ cm^2\ V^{-1}\ s^{-1}$ at 300 K.

Fig. 6 displays the optical transmittance spectra of the H_2-annealed TNO films. All transmittance spectra show an average transmittance above 70% in the visible region. Approximately 20% of light is lost due to reflection, since titania possesses a high refraction index. The band-gap (Eg) of TNO films increases with Nb content. This could originated from the Burstein-Moss effect and/or the formation of Nb_2O_5 with larger Eg ~ 3.4 eV than anatase TiO_2 [23]. Assuming indirect optical transition for anatase TiO_2, the UV-absorption edge of un-doped TiO_2 is near 3.2 eV [24], as shown in Fig. 7. For example, the absorption-edge for the post-annealed $Ti_{1-0.39}Nb_{0.39}O_2$ film, deposited at the Nb target power of 120 W, blue-shifted from 3.2 eV to 3.5 eV with increasing Nb concentration, up to 9.7 at.%. The blue-shift could be primarily caused by the well-known Burstein-Moss shift [16], which is often observed

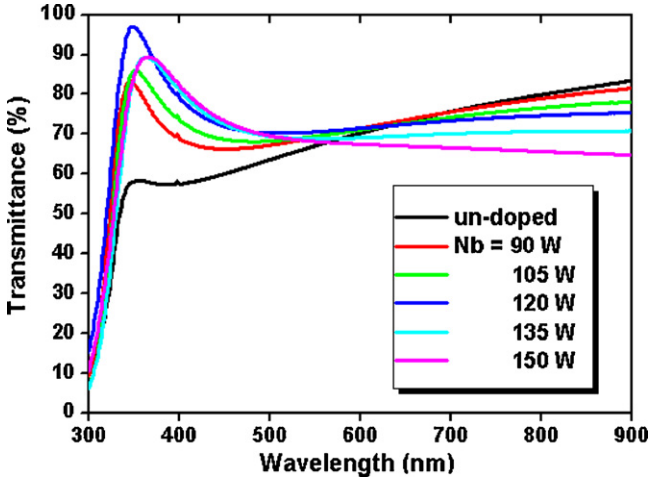

Fig. 6. Optical transmittance spectra of the H_2-annealed TNO films.

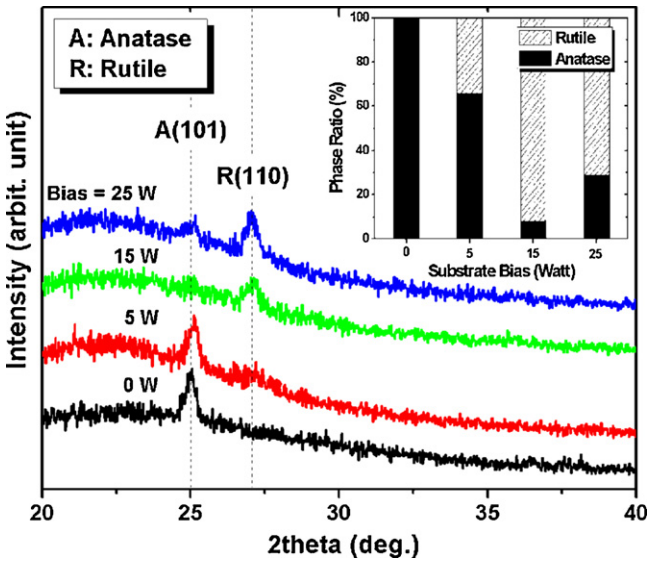

Fig. 8. X-ray diffraction patterns of the H_2-annealed TNO films deposited at various substrate bias settings. The inset shows the calculated ratio of anatase-to-rutile phase versus substrate bias.

in degenerated semiconductors, that is, the transition occurs at energies above the Fermi level, and the lowest energy conduction band is filled. Hence, photon energy increases with increasing carrier density.

The influence of ion bombardment on the structure of the TNO (Nb = 9.7 at.%) films was studied by applying substrate bias during film growth. The as-grown films in biased condition (5–25 W) were all amorphous and insulating. However, the bias effect had a significant effect on the structure of the H_2-annealed films. As shown in Fig. 8, the annealed films crystallized into either pure anatase or mixed anatase and rutile structures. The biased-TNO films showed a (1 1 0) rutile peak in the XRD spectrum, while the anatase (1 0 1) peak became weak and broad. The inset in Fig. 8 shows the calculated ratio of anatase-to-rutile phase versus substrate bias, based on the integrated peak intensities of anatase (1 0 1) and rutile (1 1 0) [25]. Consequently, the rutile content in the films is estimated to be 34% at bias = 5 W, 92% at bias = 15 W and 71% at bias = 25 W. The observed differences in crystal structure could be attributed to the potential of ionic particles such as Ti^+ and O^{2+} in plasma, which determine the crystal formation of anatase or rutile [26]. Increasing substrate bias enhances the effect of an ionized bombardment gas on the growing film surface; hence, the crystal structure and density of films could be altered by manipulating the collisions and momentum of the sputtered particles [27,28]. The as-deposited biased-TNO films, though amorphous according to XRD spectra, might contain anatase and rutile nano-grains, which upon annealing grow into large grains.

All of the biased-TNO films retained an average optical transmittance of 70% in the visible region after H_2-annealing. Nevertheless, their electrical properties were influenced by the energetic ion bombardment (Fig. 9). The subsequent heat treatment improved films electrical conductivity. Indeed, the film conductivity correlates with rutile fraction. The TNO films with the largest rutile ratio of 92%, showed the highest resistivity of $2.9 \times 10^{-1}\ \Omega$ cm; a minimum resistivity of ($1 \times 10^{-2}\ \Omega$ cm) occurred for the 34% rutile phase mix. This minimum resistivity is still one order of magnitude greater than that of the H_2-annealed films, fabricated without substrate bias ($9.2 \times 10^{-4}\ \Omega$ cm) containing only anatase phase. This implies that the fully anatase structure facilitates the carrier transport in TNO films as opposed to both amorphous of as-grown films and mixed anatase and rutile structures of annealed films.

In the mixed phase TNO films, the rutile formation suppressed the percolative conduction of anatase TNO films [29]. TiO_6 octahedra in anatase are predominantly edge-sharing, and form spiral channels through the structure for easy electron transport.

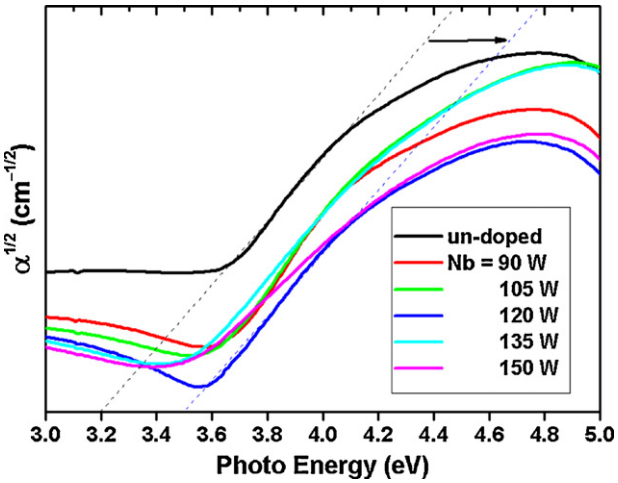

Fig. 7. Absorption coefficient as a function of photon energy for the H_2-annealed TNO films.

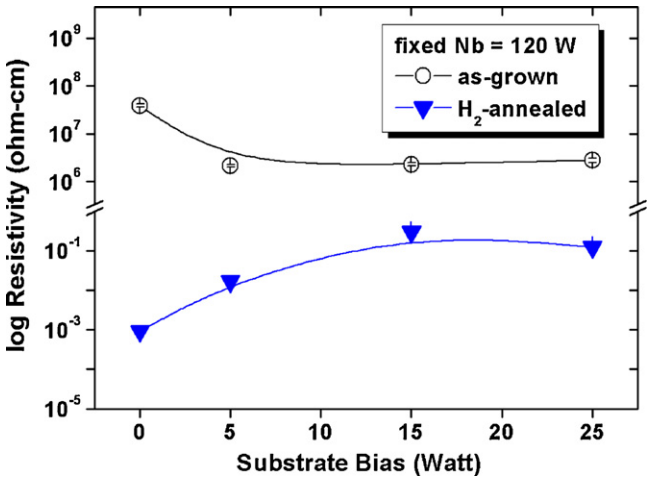

Fig. 9. Resistivity of the as-grown and the H_2-annealed TNO films prepared at various substrate bias power settings.

Additionally, the anatase structure has smaller electron effective mass ($m^* = \sim 1\, m_o$, where m_o is the electron mass), which is consistent with the observed high mobility [16]. By contrast, rutile has a large effective mass, which results in a lower Hall mobility ($m^* \sim 20\, m_o$), and its TiO_6 octahedra are mostly located at corner-sharing sites [29]. Large effective mass and corner-shared TiO_6 of rutile are unfavorable for charge carrier transport; therefore, the rutile formation suppressed the carrier transport of TNO films. Nevertheless, the TNO films of mixed anatase and rutile phases still possess a lower resistivity than that of amorphous TNO films.

In comparison with the single crystal TNO film grown on $SrTiO_3$ or $LaAlO_3$ single-crystal substrate by PLD method [8], the electrical properties of the TNO films prepared in this study are inferior due to low carrier mobility. The optimal resistivity of the single-crystal anatase $Ti_{1-x}Nb_xO_2$($x = 0.07$) is $2–3 \times 10^{-4}\ \Omega$ cm at room temperature, with a carrier density of $\sim 1 \times 10^{21}$ cm^{-3} and a mobility of ~ 22 cm^2 V^{-1} s^{-1} [8]. In contrast, the TNO films prepared in this study are $Ti_{1-x}Nb_xO_2$ (with $x = 0.25–0.52$) polycrystalline films of much higher Nb content. We speculated a few reasons that may suppress to achieve high carrier mobility of sputtered TNO. The grain size (grain boundaries), dopant, and defects like implanted Ar impurity or precipitates of second phase would affect the mobility of the TNO films. From the XRD results and SEM micrographs (not shown), it is observed that the grain size of the TNO films increase with Nb content to a certain point, approximately its solubility limit. In the annealed TNO films, some Nb content up to the solubility limit is doped in anatase lattice and the excess Nb content could form precipitates like Nb_2O_5 which could be the other source of scattering and reduce the mobility of the film. For these reasons, the defects are detrimental to high carrier mobility. Since our TNO films possess high carrier density but low carrier mobility, how to maintain high carrier density and to minimize the detrimental effects of too much dopant will be one of the keys for the TNO films of high conductivity.

4. Conclusions

Transparent conducting Nb-doped titania films with varying Nb concentrations were prepared by post-annealing reactively sputtered amorphous films. Annealing TNO films in a hydrogen reducing atmosphere caused the greatest gains in conductivity. Crystallization under H_2 atmosphere produced resistivity values, which were ten orders of magnitude lower than that of the as-deposited films. The incorporation of Nb dopant ions, formation of anatase crystalline structure, and the presence of oxygen vacancies, all contributed to a substantial reduction in resistivity in TNO films. The anatase structure has the most favorable charge-carrier transport properties when compared to either amorphous phase, or mixtures of anatase and rutile phases. The promising TNO films produced by reactive co-sputtering of Ti and Nb targets, exhibit an average transmittance of over 70% in the visible light region, a resistivity of $9.2 \times 10^{-4}\ \Omega$ cm, a carrier density of 6.6×10^{21} cm^{-3} and a mobility of 1.0 cm^2 V^{-1} s^{-1}.

Acknowledgements

Financial grant by Taiwan National Science Council under No. 96-2221-E-259-010-MY3 and the use of core-facility of Nanotechnology Center in East Taiwan are acknowledged. We thank Dr. Kola K. Rao and Dr. T.K. Chen for their useful discussions and comments on this research.

References

[1] D.S. Ginley, C. Bright, MRS Bull. 25 (2000) 15–18.
[2] K.L. Chopra, S. Major, D.K. Pandya, Thin Solid Films 102 (1983) 1–46.
[3] J.H. Noh, H.S. Han, S. Lee, D.H. Kim, J.H. Park, S. Park, J.Y. Kim, H.S. Jung, K.S. Hong, J. Phys. Chem. C 113 (2009) 1083–1087.
[4] A. Fujishima, K. Honda, Nature 238 (1972) 37–38.
[5] Y. Matsumoto, M. Murakami, T. Shono, T. Hasegawa, T. Fukumura, M. Kawasaki, P. Ahmet, T. Chikyow, S. Koshihara, H. Koinuma, Science 291 (2001) 854–856.
[6] J. Wu, X. Lu, L. Zhang, Y. Xia, F. Huang, F. Xu, J. Alloys Compd. 496 (2010) 234–240.
[7] L. Zhang, A.J. Xie, Y.H. Shen, S.K. Li, J. Alloys Compd. 505 (2010) 579–583.
[8] Y. Furubayashi, T. Hitosugi, Y. Yamamoto, K. Inaba, G. Kinoda, Y. Hirose, T. Shimada, T. Hasegawa, Appl. Phys. Lett. 86 (2005) 252101.
[9] N. Yamada, T. Shibata, K. Taira, Y. Hirose, S. Nakao, N.L. Hoang, T. Hitosugi, T. Shimada, T. Sasaki, T. Hasegawa, Appl. Phys. Express 4 (2011) 045801.
[10] R.S. Zhang, Y. Liu, Q. Gao, F. Teng, C.L. Song, W. Wang, D.R. Han, J. Alloys Compd. 509 (2011) 9178–9182.
[11] A. Roy Barman, M. Motapothula, A. Annadi, K. Gopinadhan, Y.L. Zhao, Z. Yong, I. Santoso, Ariando, M. Breese, A. Rusydi, S. Dhar, T. Venkatesan, Appl. Phys. Lett. 98 (2011) 072111.
[12] U. Takeuchi, A. Chikamatsu, T. Hitosugi, H. Kumigashira, M. Oshima, Y. Hirose, T. Shimada, T. Hasegawa, J. Appl. Phys. 107 (2010) 023705.
[13] J.Y. Kim, J.H. Noh, K. Zhu, A.F. Halverson, N.R. Neale, S. Park, K.S. Hong, A.J. Frank, ACS Nano 5 (2011) 2647–2656.
[14] M. Yang, D. Kim, H. Jha, K. Lee, J. Paul, P. Schmuki, Chem. Commun. 47 (2011) 2032–2034.
[15] X. Lu, X. Mou, J. Wu, D. Zhang, L. Zhang, F. Huang, F. Xu, S. Huang, Adv. Funct. Mater. 20 (2010) 509–515.
[16] D. Kurita, S. Ohta, K. Sugiura, H. Ohta, K. Koumoto, J. Appl. Phys. 100 (2006) 096105.
[17] S.X. Zhang, D.C. Kundaliya, W. Yu, S. Dhar, S.Y. Young, L.G. Salamanca-Riba, S.B. Ogale, R.D. Vispute, T. Venkatesan, J. Appl. Phys. 102 (2007) 013701.
[18] M.A. Gillispie, M.F.A.M. van Hest, M.S. Dabney, J.D. Perkins, D.S. Ginley, J. Appl. Phys. 101 (2007) 033125.
[19] T. Hitosugi, A. Ueda, S. Nakao, N. Yamada, Y. Furubayashi, Y. Hirose, T. Shimada, T. Hasegawa, Appl. Phys. Lett. 90 (2007) 212106.
[20] G.Q. Wang, W. Lan, G.J. Han, Y. Wang, Q. Su, X.Q. Liu, J. Alloys Compd. 509 (2011) 4150–4153.
[21] L. Sheppard, T. Bak, J. Nowotny, C.C. Sorrell, S. Kumar, A.R. Gerson, M.C. Barnes, C. Ball, Thin Solid Films 510 (2006) 119–124.
[22] S.X. Zhang, S. Dhar, W. Yu, H. Xu, S.B. Ogale, T. Venkatesan, Appl. Phys. Lett. 91 (2007) 112113.
[23] K. Yoshimura, T. Miki, S. Iwama, S. Tanemura, Thin Solid Films 281–282 (1996) 235–238.
[24] H. Tang, K. Prasad, R. Sanjinès, P.E. Schmid, F. Lévy, J. Appl. Phys. 75 (1994) 2042–2047.
[25] S.H. Kang, J.W. Lim, H.S. Kim, J.Y. Kim, Y.H. Chung, Y.E. Sung, Chem. Mater. 21 (2009) 2777–2788.
[26] A. Caballero, D. Leinen, A. Fernández, A. Justo, J.P. Espinós, A.R. González-Elipe, J. Appl. Phys. 77 (1995) 591–597.
[27] H.C. Yao, M.C. Chiu, W.T. Wu, F.S. Shieu, J. Electrochem. Soc. 153 (2006) F237–F243.
[28] W. Zhou, X. Zhong, X. Wu, L. Yuan, Q. Shu, W. Li, Y. Xia, J. Phys. D: Appl. Phys. 40 (2007) 219–226.
[29] M.A. Gillispie, M.F.A.M. van Hest, M.S. Dabney, J.D. Perkins, D.S. Ginley, J. Mater. Res. 22 (2007) 2832–2837.